

# Facile Synthesis of Three-Dimensional Pt-TiO<sub>2</sub> Nano-networks: A Highly Active Catalyst for the Hydrolytic Dehydrogenation of Ammonia-Borane

Mohammad Aref Khalily, Hamit Eren, Serdar Akbayrak, Hepi Hari Susapto, Necmi Biyikli,\* Saim Özkar,\* and Mustafa O. Guler\*

**Abstract:** Three-dimensional (3D) porous metal and metal oxide nanostructures have received considerable interest because organization of inorganic materials into 3D nano-materials holds extraordinary properties such as low density, high porosity, and high surface area. Supramolecular self-assembled peptide nanostructures were exploited as an organic template for catalytic 3D Pt-TiO<sub>2</sub> nano-network fabrication. A 3D peptide nanofiber aerogel was conformally coated with TiO<sub>2</sub> by atomic layer deposition (ALD) with angstrom-level thickness precision. The 3D peptide-TiO<sub>2</sub> nano-network was further decorated with highly monodisperse Pt nanoparticles by using ozone-assisted ALD. The 3D TiO<sub>2</sub> nano-network decorated with Pt nanoparticles shows superior catalytic activity in hydrolysis of ammonia-borane, generating three equivalents of H<sub>2</sub>.

The three-dimensional (3D) porous metal and metal oxide aerogels have recently attracted enormous interest, because assembly of bulk inorganic materials into 3D nanomaterials generates exciting features such as low density, high porosity, and high surface area.<sup>[1]</sup> Porous 3D aerogels allow rapid flow of electrons, ions, and molecules, which makes them extremely attractive for applications such as catalysis,<sup>[2]</sup> sensing,<sup>[3]</sup> fuel cells,<sup>[4]</sup> and supercapacitors.<sup>[5]</sup> Numerous techniques have been developed to prepare porous metal and metal oxide nanomaterials, including templating, combustion, cathodic corrosion, and aerogel formation.<sup>[4b]</sup> However, a significant challenge exists to synthesize metal and metal oxide 3D nanomaterials in controlled and reproducible manner. Therefore, uniform and highly controlled deposition of metals and metal oxides at ambient temperatures on soft organic templates, which can assemble into desired structures (1D, 2D, and 3D), shape and morphology, could be a promis-

ing strategy to prepare variety of porous inorganic 3D nanomaterials. Self-assembling peptides are a class of supramolecular polymers, which exploit noncovalent interactions such as hydrogen bonding, hydrophobic, electrostatic,  $\pi$ - $\pi$ , and van der Waals interactions to generate well-defined supramolecular nanostructures including nanospheres, nanosheets, nanotubes, and nanofibers.<sup>[6]</sup> These versatile supramolecular polymers can encapsulate large amounts of water to form gels, which have been extensively utilized as 2D and 3D scaffolds.<sup>[7]</sup> Critical and air-dried self-assembled peptide nanofiber gels can form self-standing porous 3D aerogels and xerogels, which are made up of highly dense 1D nanofibers. These 3D aerogels can be used as soft templates to deposit and support various inorganic nanomaterials from 1D to 3D.<sup>[8]</sup>

Atomic layer deposition (ALD) is a chemical vapor deposition technique based on sequential, self-limiting surface reactions between gaseous precursors and a solid surface to deposit materials in an atomic layer-by-layer fashion, which paves the way for controlling the film thickness and size of nanoparticles by the number of growth cycles.<sup>[9]</sup> It provides unmatched capabilities for highly uniform coating of surfaces, powders, and porous structures with a variety of materials at ambient temperatures. Furthermore, cyclic deposition nature of the ALD allows synthesis of nanoparticles with precise size and composition. Various types of well-dispersed catalysts, such as monometallic,<sup>[10]</sup> bimetallic,<sup>[11]</sup> and core-shell nanoparticles,<sup>[12]</sup> were successfully produced by ALD.

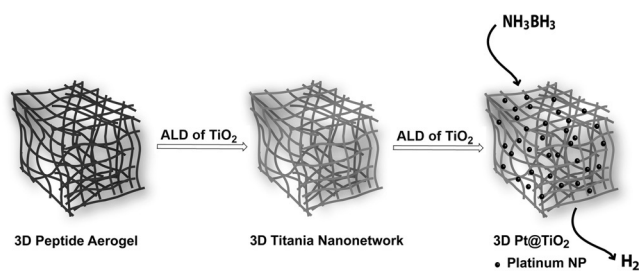
Herein, we combined advantages of two bottom-up nanofabrication techniques to engineer a novel metal/metal oxide 3D nano-network in a highly controlled manner. Self-assembling peptides were used to produce a 3D nano-network of high-aspect-ratio nanofibers as a soft organic template. The 3D peptide nanofiber aerogel was conformally coated with TiO<sub>2</sub> via ALD. The 3D peptide-TiO<sub>2</sub> nano-network was further decorated with highly monodisperse Pt nanoparticles by using ALD (Pt@TiO<sub>2</sub>, Scheme 1). These high-surface-area 3D Pt@TiO<sub>2</sub> nano-networks were utilized for hydrolysis of ammonia-borane (AB) for H<sub>2</sub> generation. Owing to its high hydrogen content (19.6 wt %), high stability in the solid state and solution under ambient conditions, nontoxicity, and high solubility,<sup>[13]</sup> AB has been considered as one of the most promising hydrogen storage materials for on-board applications.<sup>[14]</sup> We systematically studied the effect of platinum nanoparticle size on catalytic activity and found that platinum nanoparticles with size of ca. 2.4 nm provide the highest turnover frequency of 311 min<sup>-1</sup> for hydrogen generation in the hydrolysis of AB at ambient temperature.

[\*] M. A. Khalily, H. Eren, H. H. Susapto, Prof. N. Biyikli, Prof. M. O. Guler

Institute of Materials Science and Nanotechnology  
National Nanotechnology Research Center (UNAM)  
Bilkent University, Ankara 06800 (Turkey)  
E-mail: biyikli@unam.bilkent.edu.tr  
moguler@bilkent.edu.tr

S. Akbayrak, Prof. S. Özkar  
Department of Chemistry, Middle East Technical University  
Ankara 06800 (Turkey)  
E-mail: sozkar@metu.edu.tr

Supporting information and the ORCID identification number(s) for the author(s) of this article can be found under:  
<http://dx.doi.org/10.1002/anie.201605577>.



**Scheme 1.** Fabrication of 3D Pt@TiO<sub>2</sub> nano-networks via ALD.

A self-assembling peptide amphiphile molecule with a sequence of Lauryl-VVAGK-Am (K-PA; Supporting Information, Figure S1) was synthesized by using solid-phase peptide synthesis<sup>[15]</sup> and characterized by liquid chromatography–mass spectrometry (Supporting Information, Figures S2,S3). Self-assembly of K-PA molecule was studied by circular dichroism (CD) spectroscopy. The K-PA molecules were dissolved in acidic medium (pH 2) and self-assembled due to hydrophobic collapse and hydrogen bonding. The CD spectrum (Supporting Information, Figure S4a) exhibited a broad negative band at around 200 nm due to random coil structure of the K-PA molecules at acidic conditions caused by electrostatic repulsions among protonated amine groups. This band in the CD spectrum of K-PA (Supporting Information, Figure S4a) is converted into a positive peak at 195 nm and a negative band at 220 nm upon raising the pH to 10. The observed change in the CD spectrum upon charge neutralization indicated the transformation of random structure to highly ordered beta-sheets.<sup>[15]</sup>

As an intrinsic characteristic of self-assembling peptide amphiphile molecules, they can encapsulate large amount of water to form a gel. A solution of 1 wt % K-PA was converted into a self-supporting gel with a storage modulus ( $G'$ ) of 13 kPa and loss modulus ( $G''$ ) of 1.3 kPa as measured by an oscillatory rheometer (Supporting Information, Figure S4b). The K-PA gel with a damping factor ( $G''/G'$ ) of 0.01 showed dominantly elastic over viscous character.<sup>[16]</sup> A scanning electron microscope (SEM) image of critically dried K-PA aerogel revealed a 3D network of high-aspect-ratio 1D peptide nanofibers (Supporting Information, Figure S4c) with a length in micrometers and diameter of ca. 10 nm (Supporting Information, Figure S4d) as shown by transmission electron microscopy (TEM). Utilization of 3D peptide aerogels as sacrificial template to synthesize 3D metal and metal oxide aerogels offer many advantages such as tuning of porosity and surface area by simply playing with concentration of peptide gel. The 3D peptide aerogel was used as a sacrificial organic template to deposit titania by atomic layer deposition (ALD). Titania is a cheap, nontoxic, and chemically stable metal oxide, which is widely used as a support for various types of catalytic nanoparticles.<sup>[17]</sup> Deposition of 150 cycles of titania at 150 °C was optimized to grow uniform ultrathin film having  $6 \pm 1$  nm thickness (Figure 1 a,b; Supporting Information, Figure S6). Deposition of TiO<sub>2</sub> at ambient temperature is extremely crucial for preserving the skeletal structure of 3D peptide aerogel (Figure 1 a). As-prepared 3D TiO<sub>2</sub> nano-network is amor-

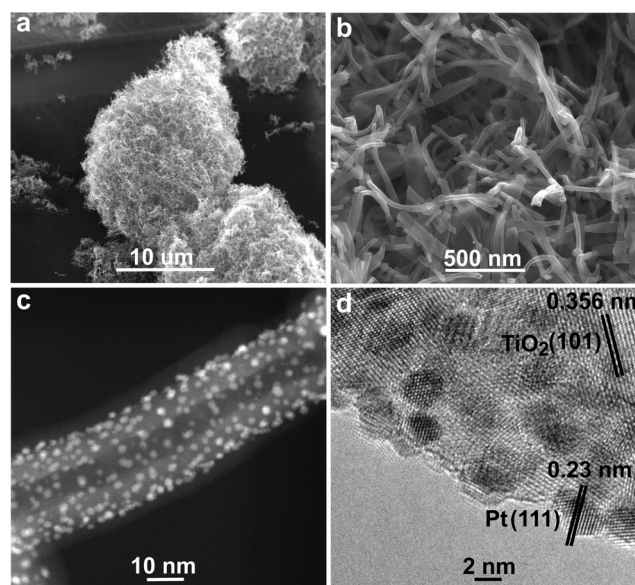


**Figure 1.** a), b) SEM images of the 3D TiO<sub>2</sub> nano-network; c) STEM and d) HRTEM images of the Pt-decorated 3D TiO<sub>2</sub> nano-network.

phous as demonstrated by powder XRD pattern (Supporting Information, Figure S5c) and has a surface area of  $45 \text{ m}^2 \text{ g}^{-1}$  as estimated from the Brunauer–Emmett–Teller (BET) analysis (Supporting Information, Figure S5d). Interestingly, the ALD not only provides highly conformal, uniform, and controlled deposition of metals and metal oxides, but also allows low-temperature growth of these nanomaterials, which makes it attractive for thermally sensitive substrates such as soft organic templates.

We utilized MeCpPtMe<sub>3</sub> as Pt precursor and O<sub>3</sub> as reactant gas to grow Pt nanoparticles with precise sizes on as-synthesized 3D TiO<sub>2</sub> nano-network (Figure 1 c). We deposited Pt with different cycles to produce 3D nano-networks containing Pt nanoparticles (Pt5@ TiO<sub>2</sub>–Pt30@ TiO<sub>2</sub>) in a controlled size ranging from 0.8 to 2.8 nm (Table 1; Supporting Information, and Figure S7a–l). Histograms (Supporting Information, Figure S7) show a very narrow range of nanoparticle size distribution. A linear increase of nanoparticle size was observed with increasing number of Pt cycles (Supporting Information, Figure S7m). Likewise, Pt loading linearly increased from 2.2% to 16% as number of Pt cycles was increased from 5 to 30 (Supporting Information, Figure S7n). The highly uniform deposition and presence of Pt nanoparticles on 3D TiO<sub>2</sub> nano-network were confirmed by STEM images and energy dispersive spectrometry (EDS), respectively (Supporting Information, Figure S8). We performed X-ray photoelectron spectroscopy (XPS) to analyze elemental composition of our nanocatalysts (Supporting Information, Figure S9). The peaks at 530, 400, and 285 eV, arising from peptide template, confirmed the presence of oxygen, nitrogen, and carbon, respectively. The signal at 458 eV is caused by TiO<sub>2</sub><sup>[8a]</sup> while peak at 73 eV showed presence of Pt species. We further conducted high-resolution XPS to analyze the electronic states of Pt species (Supporting Information, Figure S10). Deconvolution of Pt 4f bands reveals the existence of Pt<sup>0</sup>, Pt<sup>II</sup> and Pt<sup>IV</sup> species

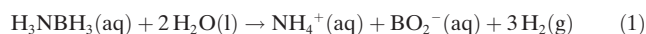
**Table 1:** Characteristics of 3D Pt@TiO<sub>2</sub> nano-networks and their turnover frequency (TOF, min<sup>-1</sup>) in hydrolysis of AB at 25.0 ± 0.1 °C.

Catalyst	ALD Pt cycle <sup>[a]</sup>	Pt loading <sup>[b]</sup> [%wt]	Particle size <sup>[c]</sup> [nm]	Binding Energy of Pt <sup>0</sup> Pt4f <sub>7/2</sub> [eV]	[Pt] <sup>[d]</sup> [mm]	TOF <sub>app</sub> [min <sup>-1</sup> ] cycle number:		
						1	2	3
Pt5@TiO <sub>2</sub>	5	2.20	0.8 ± 0.15	72.38	0.178	73	63	56
Pt10@TiO <sub>2</sub>	10	4.20	1.5 ± 0.17	71.84	0.164	171	125	108
Pt15@TiO <sub>2</sub>	15	8.50	1.8 ± 0.25	71.08	0.218	211	137	114
Pt20@TiO <sub>2</sub>	20	10.4	2.1 ± 0.32	71.03	0.231	242	201	171
Pt25@TiO <sub>2</sub>	25	13.5	2.4 ± 0.40	71.02	0.159	311	273	234
Pt30@TiO <sub>2</sub>	30	16.0	2.8 ± 0.34	72.48	0.147	174	142	126

[a] Number of Pt cycle in ALD. [b] Pt loading determined by ICP-MS. [c] Determined by TEM, which was taken from the catalyst before catalytic activity test. [d] Pt concentrations during catalysis.

(Figure S10).<sup>[18]</sup> The powder XRD pattern of Pt5@TiO<sub>2</sub> and Pt10@TiO<sub>2</sub> showed amorphous structures and no detectable Pt diffraction peaks (Supporting Information, Figure S11). Uniform spreading, low loading, and small size of Pt nanoparticles could be the reason for undetectable Pt signals in XRD. Interestingly, amorphous titania was converted into anatase (A) and rutile (R) crystal structures as the number of Pt cycle was switched from 10 to 15 and above (Supporting Information, Figure S11). Pt<sup>0</sup> nanoparticles are formed from combustion reaction of Pt precursor ligands in the presence of O<sub>3</sub>. During combustion reaction, heat given out could have caused local crystallization of TiO<sub>2</sub>. The 3D nano-networks (Pt15@TiO<sub>2</sub>-Pt30@TiO<sub>2</sub>) demonstrated a broad diffraction pattern between 38–40°. Pt (111) resonates at 39.76° and could have been overlapped with crystal plane of Ti (004) and (112).<sup>[19]</sup> Catalytic activity is highly dependent on crystal plane of the nanoparticles; therefore, we further conducted high-resolution transmission electron microscopy (HRTEM) to acquire crystal plane of Pt (Figure 1d; Supporting Information, Figure S12). The distance between two adjacent lattice fringes is about 0.23 nm, which is attributed to (111) crystal plane of fcc Pt.<sup>[20]</sup> Pt (111) is the dominant catalytic active surface for hydrolysis of ammonia-borane.<sup>[21]</sup> Highly ordered crystal patterns were also observed for TiO<sub>2</sub> (Figure 1d; Supporting Information, Figure S12), which is consistent with XRD data.

To study the catalytic activity of 3D Pt@TiO<sub>2</sub> nano-networks, we used hydrolytic dehydrogenation of ammonia-borane. Hydrolysis [Eq. (1)] is the most efficient way of releasing hydrogen from AB, which is mainly due to favorable kinetics under mild conditions.<sup>[22]</sup>



Since the reaction is required to be catalyzed at an appreciable rate at ambient temperature, developing efficient and stable catalysts for hydrogen generation from AB is a challenge for fuel cell applications. Although various supported transition metal nanoparticles have been tested for H<sub>2</sub> generation from the hydrolysis of ammonia-borane,<sup>[23]</sup> Pt has been shown to be the superior catalyst.<sup>[21,24]</sup> However, high price and low abundance of Pt in the Earth crust limit its catalytic application. Therefore, synthesis of Pt nanoparticles with controlled size and desired crystal lattice plane is of importance for reducing the cost by efficient use of Pt

catalyst. Moreover, uniform deposition of Pt nanoparticles on high-surface-area 3D nano-network support can further boost reaction kinetics by allowing rapid diffusion of reactants through 3D support, which possibly will improve substrate-catalyst interactions. Therefore, 3D Pt@TiO<sub>2</sub> nano-network can be an efficient catalyst to generate H<sub>2</sub> from AB.

The 3D TiO<sub>2</sub> nano-network is shown to be inactive in H<sub>2</sub> generation from the hydrolysis of AB at room temperature. However, the 3D Pt@TiO<sub>2</sub> nano-networks are found to be highly active in the hydrolysis of AB generating 3.0 equivalents of H<sub>2</sub> per mole of AB under the same conditions. The 3D Pt@TiO<sub>2</sub> nano-networks with different particle size and Pt loading were fabricated by varying the number of ALD cycles and tested in H<sub>2</sub> generation from the hydrolysis of AB. Plots of time dependent H<sub>2</sub> production per mole of catalyzed by 3D Pt@TiO<sub>2</sub> nano-network with varying metal loading at 25.0 ± 0.1 °C are shown in the Supporting Information, Figure S13. In all cases, H<sub>2</sub> evolution starts immediately without an induction period, a consequence of using preformed catalyst, and continues almost linearly until the consumption of all of the AB present in the solution. The turnover frequency (TOF), calculated from the hydrogen generation rate in the linear portion of each plot, shows variation with the number of ALD cycles (Table 1; Supporting Information, Figure S13g) and with the size of Pt nanoparticles (Table 1; Supporting Information, Figure S13h). The volcano curve of activity versus the Pt particle size suggests that the (111) facets of Pt@TiO<sub>2</sub> nanocatalyst are dominating active sites with some contribution from (100) facets.<sup>[21]</sup> The increase in the catalytic activity of 3D Pt@TiO<sub>2</sub> nanocatalyst with the number of ALD cycles up to 25 correlates well with the decrease in the Pt 4f<sub>7/2</sub> binding energy (Table 1; Supporting Information, Figure S10). As the number of ALD cycles increases the Pt<sup>0</sup> 4f<sub>7/2</sub> bands shift to the lower energy values, which indicates higher electron transfer from the surface oxygen to Pt.<sup>[25]</sup> It is conceivable that the electron transfer increases with increasing surface interaction of Pt nanoparticles and oxide surface of titania as nanoparticles become larger. Note that the crystallinity of titania surface also increases with the increasing number of ALD cycles, which might be induced by the same surface interaction. The Pt25@TiO<sub>2</sub> nanocatalyst with 25 Pt ALD cycles (2.4 nm Pt nanoparticle size and 13.5% Pt loading) provides the highest catalytic activity, with a TOF value of 311 min<sup>-1</sup> in H<sub>2</sub> generation from the hydrolysis of AB at 25.0 ± 0.1 °C



(Table 1; Supporting Information, Figure S13e). TOF values of the reported Pt catalysts used in the hydrolysis of AB are listed in the Supporting Information, Table S1 for comparison. More clearly seen from the TOF values, Pt25@TiO<sub>2</sub> (311 min<sup>-1</sup>) has approximately three times greater catalytic activity than that of commercial Pt/C catalyst (111 min<sup>-1</sup>). Furthermore, Pt25@TiO<sub>2</sub> shows higher catalytic activity than most of the Pt-based catalysts such as Pt/ $\gamma$ -Al<sub>2</sub>O<sub>3</sub>, Pt/CeO<sub>2</sub>, Ni<sub>0.33</sub>@Pt<sub>0.67</sub>/C, Co<sub>0.32</sub>Pt<sub>0.68</sub>/C, Pt cube/CeO<sub>2</sub>/RGO, Pt/SiO<sub>2</sub>, and PtRu/C (Supporting Information, Table S1). However, the catalytic activity of Pt25@TiO<sub>2</sub> is slightly lower than that of Pt/CNTs-*O*-HT and Pt@MIL-101. The lower catalytic activity of Pt25@TiO<sub>2</sub> compared to Pt/CNTs-*O*-HT and Pt@MIL-101 may be attributed to the lower surface area of 3D titania nano-network (45 m<sup>2</sup>g<sup>-1</sup>) as compared to that of carbon nanotubes (221 m<sup>2</sup>g<sup>-1</sup>) and metal-organic frameworks (5900 m<sup>2</sup>g<sup>-1</sup>). The durability of 3D Pt@TiO<sub>2</sub> nanocatalysts was tested by recycling experiment (Table 1); when AB is completely hydrolyzed, another batch of AB is added for the next run of hydrolysis. The Pt25@TiO<sub>2</sub> nanocatalyst retains at least 87 % of its initial activity in the second cycle and 75 % in the third cycle (Table 1). The decrease in the catalytic activity can be attributed to the agglomeration of Pt nanoparticles as shown by STEM images taken after recycling experiments (Supporting Information, Figure S14) and to the deactivation effect of the hydrolysis product metaborate, which accumulates during the hydrolysis. We further analyzed and compared the electronic properties of the fresh catalyst with the recycled catalyst (Supporting Information, Figure S15). The fresh Pt25@TiO<sub>2</sub> catalyst contains 23.59 % Pt<sup>0</sup> species, while the deactivated catalyst contains 12.68 % Pt<sup>0</sup>. The drastic decrease in Pt<sup>0</sup> content is another reason for the decrease in catalytic activity of catalyst after recycling. Previous studies have shown that agglomeration/sintering of nanoparticles can be efficiently prevented by atomic layer deposition technique. Deposition of thin layers of Al<sub>2</sub>O<sub>3</sub> on supported Pd nanoparticles<sup>[26]</sup> and thin layers of TiO<sub>2</sub> on supported Co nanoparticles<sup>[27]</sup> prevented agglomeration/sintering, therefore improving the lifetime of nanocatalysts to a great extent. This is another striking advantage of the ALD. We further measured the leaching of Pt nanoparticles from 3D Pt@TiO<sub>2</sub> nano-network after the third use. The ICP-MS results demonstrated that Pt leached less than 0.1 %, which confirmed strong anchoring of Pt nanoparticles on 3D TiO<sub>2</sub> nano-networks.

In summary, we exploited a self-assembled peptide nanofiber 3D aerogel as a template to fabricate highly uniform, conformal, and porous 3D TiO<sub>2</sub> nano-networks. The 3D TiO<sub>2</sub> nano-networks were further decorated by Pt nanoparticles with controlled and precise size using ozone-assisted ALD technique. Pt particle size and loadings were tuned by altering the number of Pt ALD cycles. The Pt25@TiO<sub>2</sub> with ca. 2.4 nm particle size showed superior catalytic activity in H<sub>2</sub> generation from AB with a TOF value of 311 min<sup>-1</sup> at room temperature. Moreover, Pt leaching was fairly low from 3D Pt@TiO<sub>2</sub> nano-networks. Combination of supramolecular peptide nanofiber 3D templates with ALD technique allows facile, straightforward, and highly reproducible preparation of metal, metal oxide, and semiconductor 3D nanomaterials

as next-generation nanocatalysts with light weight, high-surface-area and porosity.

## Acknowledgements

This work was supported partially supported by TUBITAK grant number 112M578 and Turkish Academy of Sciences.

**Keywords:** 3D nanomaterials · ammonia–borane · atomic layer deposition · hydrogen generation · peptide aerogels

**How to cite:** *Angew. Chem. Int. Ed.* **2016**, *55*, 12257–12261  
*Angew. Chem.* **2016**, *128*, 12445–12449

- [1] a) W. Liu, A. K. Herrmann, N. C. Bigall, P. Rodriguez, D. Wen, M. Oezaslan, T. J. Schmidt, N. Gaponik, A. Eychmuller, *Acc. Chem. Res.* **2015**, *48*, 154–162; b) S. Sánchez-Paradinas, D. Dorfs, S. Friebe, A. Freytag, A. Wolf, N. C. Bigall, *Adv. Mater.* **2015**, *27*, 6152–6156; c) C. Z. Zhu, D. Du, A. Eychmuller, Y. H. Lin, *Chem. Rev.* **2015**, *115*, 8896–8943.
- [2] D. Wen, A. K. Herrmann, L. Borchardt, F. Simon, W. Liu, S. Kaskel, A. Eychmuller, *J. Am. Chem. Soc.* **2014**, *136*, 2727–2730.
- [3] J. T. Korhonen, P. Hiekkataipale, J. Malm, M. Karppinen, O. Ikkala, R. H. A. Ras, *ACS Nano* **2011**, *5*, 1967–1974.
- [4] a) W. Liu, A. K. Herrmann, D. Geiger, L. Borchardt, F. Simon, S. Kaskel, N. Gaponik, A. Eychmuller, *Angew. Chem. Int. Ed.* **2012**, *51*, 5743–5747; *Angew. Chem.* **2012**, *124*, 5841–5846; b) W. Liu, P. Rodriguez, L. Borchardt, A. Foelske, J. P. Yuan, A. K. Herrmann, D. Geiger, Z. K. Zheng, S. Kaskel, N. Gaponik, R. Kotz, T. J. Schmidt, A. Eychmuller, *Angew. Chem. Int. Ed.* **2013**, *52*, 9849–9852; *Angew. Chem.* **2013**, *125*, 10033–10037.
- [5] A. Mahmood, R. Q. Zou, Q. F. Wang, W. Xia, H. Tabassum, B. Qiu, R. Zhao, *ACS Appl. Mater. Interfaces* **2016**, *8*, 2148–2157.
- [6] X. B. Zhao, F. Pan, H. Xu, M. Yaseen, H. H. Shan, C. A. E. Hauser, S. G. Zhang, J. R. Lu, *Chem. Soc. Rev.* **2010**, *39*, 3480–3498.
- [7] E. Arslan, I. C. Garip, G. Gulseren, A. B. Tekinay, M. O. Guler, *Adv. Healthcare Mater.* **2014**, *3*, 1357–1376.
- [8] a) H. Ceylan, C. Ozgit-Akgun, T. S. Erkal, I. Donmez, R. Garifullin, A. B. Tekinay, H. Usta, N. Biyikli, M. O. Guler, *Sci. Rep.* **2013**, *3*, 2306; b) M. A. Khalily, O. Ustahuseyin, R. Garifullin, R. Genc, M. O. Guler, *Chem. Commun.* **2012**, *48*, 11358–11360.
- [9] J. Hämäläinen, M. Ritala, M. Leskelä, *Chem. Mater.* **2014**, *26*, 786–801.
- [10] J. S. King, A. Wittstock, J. Biener, S. O. Kucheyev, Y. M. Wang, T. F. Baumann, S. K. Giri, A. V. Hamza, M. Baeumer, S. F. Bent, *Nano Lett.* **2008**, *8*, 2405–2409.
- [11] S. T. Christensen, H. Feng, J. L. Libera, N. Guo, J. T. Miller, P. C. Stair, J. W. Elam, *Nano Lett.* **2010**, *10*, 3047–3051.
- [12] S. F. Xie, S. I. Choi, N. Lu, L. T. Riling, J. A. Herron, L. Zhang, J. Park, J. G. Wang, M. J. Kim, Z. X. Xie, M. Mavrikakis, Y. N. Xia, *Nano Lett.* **2014**, *14*, 3570–3576.
- [13] a) P. Chen, Z. T. Xiong, J. Z. Luo, J. Y. Lin, K. L. Tan, *Nature* **2002**, *420*, 302–304; b) F. Durap, M. Zahmakiran, S. Ozkar, *Appl. Catal. A* **2009**, *369*, 53–59.
- [14] A. Staubitz, A. P. M. Robertson, I. Manners, *Chem. Rev.* **2010**, *110*, 4079–4124.
- [15] M. A. Khalily, G. Gulseren, A. B. Tekinay, M. O. Guler, *Bioconjugate Chem.* **2015**, *26*, 2371–2375.
- [16] M. A. Khalily, M. Goktas, M. O. Guler, *Org. Biomol. Chem.* **2015**, *13*, 1983–1987.
- [17] S. Chaturvedi, P. N. Dave, N. K. Shah, *J. Saudi Chem. Soc.* **2012**, *16*, 307–325.

- [18] a) J. Dendooven, R. K. Ramachandran, K. Devloo-Casier, G. Rampelberg, M. Filez, H. Poelman, G. B. Marin, E. Fonda, C. Detavernier, *J. Phys. Chem. C* **2013**, *117*, 20557–20561; b) C. R. Parkinson, M. Walker, C. F. McConville, *Surf. Sci.* **2003**, *545*, 19–33.
- [19] H. Hua, C. G. Hu, Z. H. Zhao, H. Liu, X. Xie, Y. Xi, *Electrochim. Acta* **2013**, *105*, 130–136.
- [20] Q. M. Shen, L. P. Jiang, H. Zhang, Q. H. Min, W. H. Hou, J. J. Zhu, *J. Phys. Chem. C* **2008**, *112*, 16385–16392.
- [21] W. Y. Chen, J. Ji, X. Feng, X. Z. Duan, G. Qian, P. Li, X. G. Zhou, D. Chen, W. K. Yuan, *J. Am. Chem. Soc.* **2014**, *136*, 16736–16739.
- [22] a) S. Akbayrak, S. Ozkar, *ACS Appl. Mater. Interfaces* **2012**, *4*, 6302–6310; b) W. Chen, D. Li, Z. Wang, G. Qian, Z. Sui, X. Duan, X. Zhou, I. Yeboah, D. Chen, *AIChE J.* **2016**, DOI: 10.1002/aic.15389.
- [23] M. Zahmakıran, S. Özkar, *Nanoscale* **2011**, *3*, 3462–3481.
- [24] A. Aijaz, A. Karkamkar, Y. J. Choi, N. Tsumori, E. Ronnebro, T. Autrey, H. Shioyama, Q. Xu, *J. Am. Chem. Soc.* **2012**, *134*, 13926–13929.
- [25] W. Y. Chen, J. Ji, X. Z. Duan, G. Qian, P. Li, X. G. Zhou, D. Chen, W. K. Yuan, *Chem. Commun.* **2014**, *50*, 2142–2144.
- [26] J. L. Lu, B. S. Fu, M. C. Kung, G. M. Xiao, J. W. Elam, H. H. Kung, P. C. Stair, *Science* **2012**, *335*, 1205–1208.
- [27] J. C. Lee, D. H. K. Jackson, T. Li, R. E. Winans, J. A. Dumesic, T. F. Kuech, G. W. Huber, *Energy Environ. Sci.* **2014**, *7*, 1657–1660.

Received: June 8, 2016

Revised: July 28, 2016

Published online: September 6, 2016